ACCSCIENCE PUBLISHING

Materials Science in Additive Manufacturing

ORIGINAL RESEARCH ARTICLE

Development of 3D-printable concrete with coarse biochar as a natural aggregate supplement

Suvash Chandra Paul*, Jihye Jhun, Junghyun Lee, Pengyu Chen, Yi Wei Daniel Tay, and Ming Jen Tan*

Singapore Centre for 3D Printing, School of Mechanical & Aerospace Engineering, Nanyang Technological University, 50 Nanyang Avenue, Singapore

Abstract

This research investigates the use of biochar as a supplement to natural aggregates in the development of 3D-printable concrete. Most studies on 3D concrete printing (3DCP) have focused on fine aggregates due to limitations in the printing system, particularly regarding the material delivery process. Pumping 3D-printable concrete with large aggregates poses challenges, as it requires larger nozzles and higher print speeds to accommodate the flow from the larger pumps, which typically have a higher flow rate than those used for fine aggregate materials. In this study, coarse biochar with a maximum size of approximately 10 mm was incorporated alongside natural coarse aggregates at volumes of 0%, 5%, and 10%. Various tests were conducted, including assessments of buildability, rheology, mechanical strength, and thermogravimetric analysis for carbon capture of the 3D-printable biochar materials, which were compared to reference materials without biochar. The findings showed that coarse biochar can effectively enhance early-age carbon sequestration while preserving printability. Although the addition of biochar reduced mechanical strength, a 5% biochar replacement achieved higher buildability. While biochar has traditionally been explored as a cement replacement or filler, its use as coarse aggregate in 3DCP is relatively new and has not been previously studied. Optimizing biochar derived from agricultural waste in concrete can further enhance the sustainability of current 3DCP technology. This approach provides a scalable strategy for integrating carbon capture functionality into digital construction materials.

Keywords: Biochar; 3D concrete printing; Buildability; Carbon capture; Mechanical strength

***Corresponding authors:**
Suvash Chandra Paul
(suvash.cp@ntu.edu.sg);
Ming Jen Tan
(mmjtan@ntu.edu.sg)

Citation: Paul SC, Jhun J, Lee J, Chen P, Tay YWD, Tan MJ. Development of 3D-printable concrete with coarse biochar as a natural aggregate supplement. *Mater Sci Add Manuf.* 2026;5(3):026190040. doi: 10.36922/MSAM026190040

Received: May 6, 2026

Revised: May 29, 2026

Accepted: June 7, 2026

Published online: July 15, 2026

1. Introduction

Driven by the growing demand for efficiency, cost reduction, and high precision in industrial production, additive manufacturing (commonly referred to as 3D printing) has become one of the most prominent advanced fabrication technologies worldwide.[1] Its flexibility enables the rapid creation of complex geometries with high accuracy. Consequently, 3D printing has found widespread applications in fields such as aerospace, biomedical engineering, functional material processing, and food production.[2-5] Recently, the construction industry has also begun adopting 3D printing,[6] recognizing its potential for fabricating intricate architectural designs that are difficult or impossible to realize using conventional techniques.[7]

Successful 3D concrete printing (3DCP) relies on cement-based materials possessing key fresh-state properties: extrudability, flowability, and buildability.[8] Extrudability refers to the material's ability to pass through equipment components like pipes and nozzles without causing blockages.[9] Flowability, often linked to deliverability or pumpability, ensures a consistent and uninterrupted material flow during printing.[10] Buildability is the material's capacity to hold its shape and support subsequent layers without deforming or collapsing immediately after extrusion.[11]

Despite progress in 3DCP, the continued dependence on traditional Ordinary Portland Cement (OPC) poses considerable environmental concerns. OPC production accounts for approximately 5–7% of global anthropogenic CO_2 emissions,[12] with an annual production of about 4.4 billion metric tons in 2021.[13] To improve the sustainability of 3D printing in construction, the development of alternative, low-carbon-emission binders and aggregates is crucial for reducing emissions and potentially enabling carbon capture in a sustainable manner.

Biochar, a carbon-rich byproduct of waste biomass pyrolysis, has gained significant interest for its potential in climate change mitigation and as a sustainable additive or partial aggregate replacement in cement-based materials.[14,15] Pyrolysis of lignocellulosic waste biomass shows potential for altering concrete properties under both normal and elevated temperatures. During pyrolysis, the escape of biomass volatiles creates a wide range of pores in biochar. This porous nature of biochar is believed to benefit concrete, particularly in resisting thermal damage, as fine biochar particles can reduce permeability and mitigate pore-pressure buildup at elevated temperatures.[16]

An existing study reported that adding 2% (by cement wt.) fine biochar, prepared from wood or mixed food waste at 500 °C, to cement mortar improved mechanical strength by 20–25% compared to a reference mix.[17] Pre-soaked biochar was found to perform better than dry biochar. Long-term studies (up to 2 years) further confirmed that biochar-added concrete exhibited higher strength at a 2% cement replacement level, with results at 5% replacement still comparable to reference concrete.[18] It is hypothesized that water trapped in the porous biochar during mixing can gradually release, thereby sustaining hydration reactions and strength development. However, an excess amount of biochar can decrease concrete strength because biochar particles are relatively lighter than traditional cement or aggregate, impacting the concrete mass due to their low particle density. A water absorption test on concrete samples showed approximately 3.64% lower absorption in 5% biochar-added concrete mixes compared to the reference mix over 7 days of testing.[18]

Biochar types and pyrolysis temperature also play important roles in concrete properties.[19] Food waste-digested (FWD) biochar performed better than wood waste-derived (WWD) biochar, attributed to its lower pore volume and critical entry radius. Similarly, concrete strength increased with pyrolysis temperature, from 550 °C to 750 °C. This enhanced strength was attributed to the higher ash content and micro-strength of FWD biochar compared to WWD biochar. Mercury intrusion porosimetry (MIP) tests also confirmed the formation of more pores in biochar at higher temperatures. Furthermore, dissolved ions from biochar were detected, which are believed to influence cement hydration and improve strength, even at higher pyrolysis temperatures.[19]

Incorporating biochar into cementitious materials not only reduces the consumption of tradition binders and aggregates but also contributes to carbon sequestration by trapping atmospheric CO_2 within the concrete matrix throughout its lifecycle.[20] Although research on large-sized biochar in concrete production is limited, a study[21] converted biochar into carbon-rich lightweight aggregates (C-LWA) with a grain size of 8–20 mm. These C-LWAs were then used to replace natural coarse aggregates in concrete production. While the resulting concrete exhibited reduced strength, carbon analysis confirmed that the C-LWAs compensated for the high CO_2 emissions inherent in concrete production. Notably, concretes containing C-LWA achieved net-zero emissions.[21] Its porous structure and high surface area enable biochar to enhance internal curing, reduce density, and improve thermal insulation, while offering the environmental advantage of negative carbon emissions.[22] In concrete, biochar facilitates water retention, supports internal curing, and provides active sites for CO_2 absorption,[23] features that collectively improve long-term carbon sequestration performance. Fine biochar in cementitious material can act as an internal curing agent and a nucleation site, rather than providing pozzolanic reactions, especially when used at low substitution levels.[24] Recent studies have explored the integration of biochar in both conventional casting and 3D printing, highlighting its potential to enhance the eco-efficiency of construction materials. In 3D printing applications, biochar-modified concrete can maintain adequate fresh-state properties and reduce weight due to its lower density, all while contributing to long-term CO_2 storage.[25] Furthermore, the inherent design freedom of 3D printing allows for structures with optimized surface area-to-volume ratios, potentially enhancing gas exchange and promoting further carbonation reactions within the matrix.[26]

However, the amount of supplementary cementitious materials and aggregates that can be added to concrete production is limited, as excessive amounts can negatively impact concrete properties. Existing studies on 3DCP have shown that using biochar powder up to 10% by weight of cement can improve buildability and printing accuracy without significantly affecting early strength.[26,27] Higher amounts, however, may reduce mechanical performance due to increased porosity in the matrix.[27] To address this, some researchers suggest combining biochar with CO_2 curing to balance strength and CO_2 uptake,[28,29] noting that the large porosity in biochar can enhance carbonation more uniformly, while fine porosity can improve the early-age strength of concrete.[29] These results indicate that biochar holds considerable promise for producing low-carbon, printable concrete.

Despite the growing interest in biochar-enhanced concrete, most existing studies focus on the incorporation of fine biochar particles (typically ranging from 10 μm to 500 μm) as partial replacements for cement or fine aggregates in traditional cast concrete production.[30,31] Comparatively little attention has been paid to coarse or large-particle biochar and its behavior in layer-by-layer printing. Therefore, this research aims to evaluate both the fresh and hardened properties of coarse biochar-mixed 3DCP and to explore a new approach for carbon-negative concrete construction.

While existing studies have demonstrated biochar's positive effects on mechanical strength, shrinkage, and durability, the carbon sequestration potential of biochar, particularly coarse biochar aggregates, remains underexplored. The use of fine biochar is often limited due to the adverse effects of higher volumes on workability, strength, or printability.[27] Furthermore, conventional research often focuses on cast concrete, where dense packing restricts the pore connectivity needed for effective CO_2 diffusion and long-term uptake. Optimizing particle size distribution and aggregate grading for 3D printing, where material behavior differs significantly from traditional casting, has also received limited attention.

This study proposes a novel approach using coarse biochar (maximum particle size around 10 mm) combined with coarse aggregates (6–10 mm) in 3D-printable concrete mixtures. This strategy aims to create a lightweight, highly porous structure that enhances CO_2 uptake and sequestration without compromising the fresh-state properties essential for 3D printing, such as extrudability and buildability. Incorporating larger biochar particles increases the overall biochar content and promotes internal pathways for gas exchange, facilitating continuous carbonation throughout the printed structure's service life. By leveraging the design flexibility of additive manufacturing, this method addresses the limitations of conventional dense concrete systems and offers a sustainable solution for carbon-negative construction materials. This research fills a gap in current studies by systematically investigating the balance between mechanical performance, printability, and enhanced carbon sequestration through optimized material design using macro-sized biochar and natural aggregate blends.

2. Materials and methods

2.1. Materials and mix design

This section details the experimental procedures and materials used to evaluate the printability, mechanical strength, and carbon uptake performance of a 3D-printed concrete mix incorporating coarse biochar. The biochar was incorporated by volume, replacing natural coarse aggregates at levels of 0%, 5%, and 10%. This replacement ratio was selected based on the assumption that increasing the amount of biochar in the mix would reduce the density of the concrete, potentially affecting its strength. The mix design consisted of OPC (CEM-I, Engro), undensified silica fume from Elkem, Singapore, a polycarboxylate-based superplasticizer, natural river sand (maximum particle size: 2 mm), and natural coarse aggregates (size ranges from 6 mm to 10 mm). Figure 1A presents the particle size distribution for all aggregate types used in this study. The percentage of passing for each aggregate type was determined using a CAMSIZER 3D particle size analyzer. All dry components were initially blended in a concrete planetary mixer at low speed for 3 minutes. Water and superplasticizer were then slowly added, and the entire mixture was blended at a higher speed for an additional 3–5 minutes until a homogeneous consistency was achieved. Since the biochar is highly porous and absorbs water, a pre-wetting test was conducted to determine its water absorption capacity; this value was then factored into the total mix water content. Volume-based replacement ratios were chosen because the biochar exhibited a low bulk density (approximately 300 kg/m^3) and a high-water absorption rate (approximately 20%). A weight-based replacement would have resulted in a disproportionately large volume of biochar in the mixture due to its low density. Such an excess could significantly increase the overall porosity, weaken the internal structure, and substantially reduce mechanical strength in the samples. Furthermore, the coarse size and lightweight nature of biochar could lead to poor pumpability and a higher risk of nozzle or pipe blockage during extrusion. Therefore, a volume-based replacement method was selected to ensure better control over particle distribution, maintain workable rheology, and minimize adverse effects on print quality and mechanical performance. The specific mix proportions for the biochar-incorporated 3D-printable materials are detailed in Table 1.

2.2. Printing setup and mechanical test samples

A KUKA 6-axis robotic arm, acting as a 3D printer, was used with a control system capable of printing structures up to approximately 3 m in diameter and 4 m in height, as shown in Figure 1B. The printer employed a 50 mm diameter nozzle and extruded material at a constant printing speed of 150 mm/s. To ensure uniform material deposition, a consistent layer height of 33 mm was maintained for all prints. Two distinct print patterns were used: one to assess buildability and another for the mechanical testing of printable materials (see Figure 2). Buildability was evaluated by printing a cylindrical structure with a 500 mm diameter as shown in Figure 2A, continuously depositing a single-wall spiral layer until collapse. To evaluate the buildability of the fresh materials, the maximum number of printed layers that could be stacked before failure was determined. This simulates the increasing vertical stress that accumulates during the layer-by-layer 3D printing process and compares it to the material's yield strength.

For mechanical testing, beam samples measuring approximately 1300 mm long, 100 mm wide, and 100 mm high were printed using a straight-line pattern as displayed in Figure 2B and 2C. These beams were then cut into samples for compressive and flexural strength tests, resulting in approximate cube sizes of 100 mm^3 and beams measuring 100 mm × 100 mm × 320 mm as shown in Figure 2D. To simulate typical field construction environmental conditions, all samples were cured under

Table 1. Compositions of the materials for different mixes

Mix ID	Cement (wt.%)	Silica fume (wt.%)	Sand (wt.%)	Coarse aggregate (wt.%)	Biochar (wt.%)	W/B [a]	SP/W [b]
Control	30.88	3.10	43.89	22.13	0	0.38	0.014
BC5	30.64	3.07	43.54	21.96	0.79	0.39	0.014
BC10	29.31	3.10	43.83	22.10	1.66	0.41	0.014

Notes: [a] W/B: water-binder ratio; [b] SP/W: superplasticizer-water ratio.

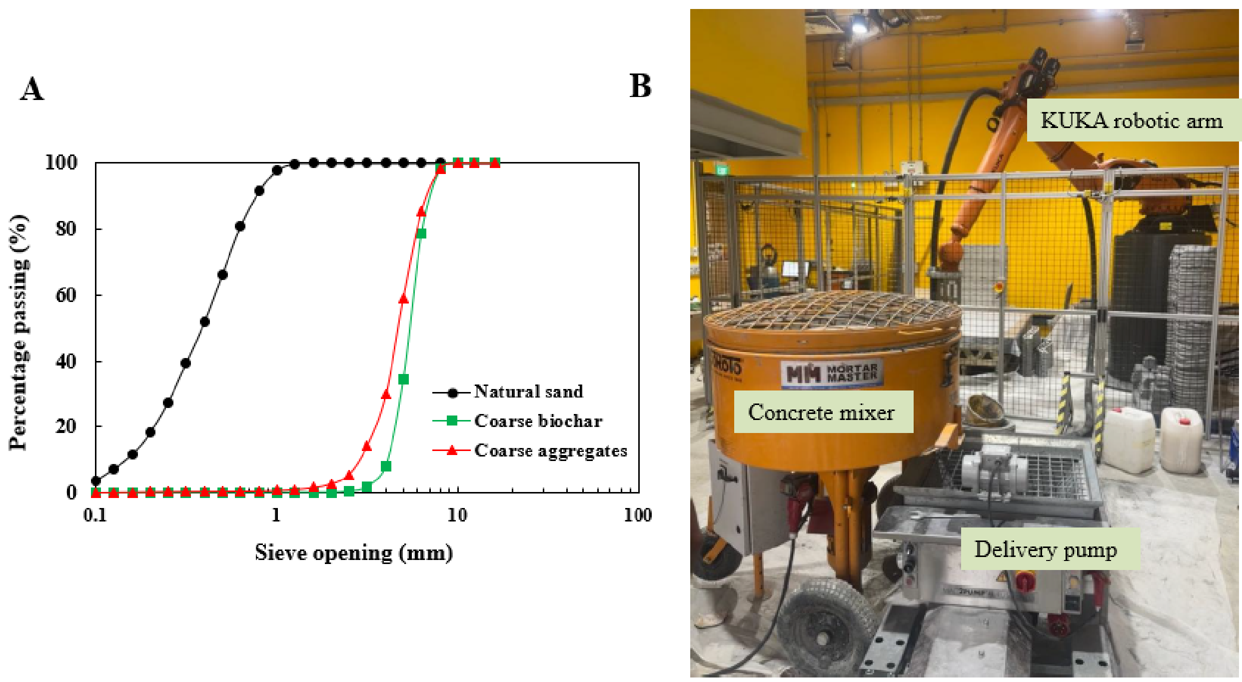

Figure 1. Particle size of the different aggregates (A) and 3D printing system used in this study (B)

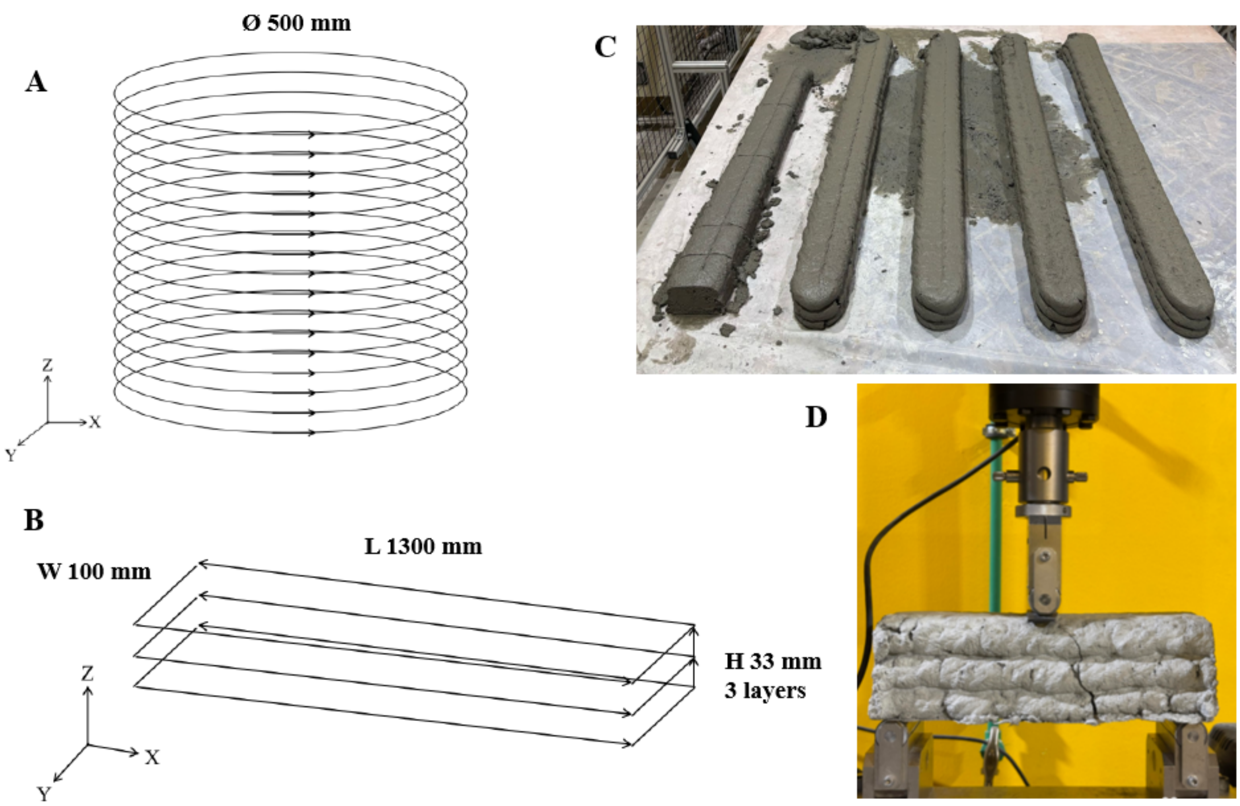

Figure 2. Tool paths and 3D-printed samples for mechanical and buildability tests. (A) Buildability tool path; (B) mechanical testing tool path; (C) printed beam samples; and (D) beam samples under flexural testing.

open-air conditions in the laboratory at controlled temperature of 21 ± 2°C and 55 ± 5% relative humidity for either 7 or 28 days.

Flexural strength was determined using a three-point bending test performed on an Instron machine with a loading rate of 0.50 mm/min and a support span of 270 mm. After flexural failure, the fractured segments were trimmed to 100 mm lengths using a mechanical cutter and then tested for compressive strength. These compressive tests were conducted using an ALFA compression testing machine, with a load applied along the Z-axis at a rate of 2.2 kN/sec to replicate vertical stress encountered in structural applications.

2.3. Rheology testing

The rheological properties of the fresh mixtures were assessed using an Anton Paar Modular Compact Rheometer. This test evaluated the material's viscoelastic behavior by measuring the storage modulus (G') and loss modulus (G"), which represent the elastic (solid-like) and viscous (liquid-like) responses, respectively. These parameters indicate the material's capacity to maintain structural integrity while flowing under external stress.

To assess thixotropic behaviour and structural recovery, a three-interval time sweep protocol was applied. First, a low strain amplitude of 0.1% at a constant frequency of 1 Hz was used to measure the initial steady-state structure.[32] Second, a high strain amplitude of 3% was applied to simulate the shear conditions during extrusion and disrupt the internal structure. Finally, the strain amplitude was returned to 0.1% to evaluate the material's structural recovery over time.

The rheological analysis was performed using a rheometer equipped with a vane spindle (height: 40 mm; radius: 15 mm) and a cylindrical container (height: 100 mm; radius: 35 mm). Each sample was measured three times, and data were logged at 5-second intervals. Key rheological indicators such as storage modulus (G'), loss modulus (G"), loss factor (tan δ), and complex viscosity (η*) were then calculated using established rheological models[33] according to **Equations 1–4**.

$$G' = G^{*}\cos\delta \quad (1)$$

$$G'' = G^{*}\sin\delta \quad (2)$$

$$\tan\delta = G^{"} / G^{'} \quad (3)$$

$$\eta^{*} = G^{*} / \omega \quad (4)$$

where G* is the complex shear modulus, δ is the phase angle, ω represents the angular frequency, and η* refers to the complex viscosity.

2.4. Prediction of buildable layers

The uniaxial unconfined compressive test (UUCT) was performed to determine the theoretical, or predicted, number of buildable layers for different concrete mixes. This test simulated the stress conditions of vertical stacking to predict the maximum number of printable layers achievable before structural failure. The test's load rate, *R*, corresponded the settlement stress growth rate during printing, derived from printing path length (*L*), printing speed (*v*), layer height (*h*), material density (ρ), and gravitational acceleration (*g*), as shown in **Equations 5–8**. This ensured the compressive stress increase per unit time matched the theoretical vertical stress increase caused by the printed structure's self-weight. The critical printable height was then determined as the point where stress exceeded the material's yield strength.

$$R = \frac{dF}{dt} \quad (5)$$

$$t_{layer} = \frac{L}{v} \quad (6)$$

$$\frac{d\sigma_s}{dt} = \rho g \frac{dh}{dt} \quad (7)$$

$$\frac{dF}{dt} = A \cdot \frac{d\sigma_s}{dt} \quad (8)$$

Here, *A* represents the contact area of the tested sample. Samples were prepared by pouring the fresh mix into PLA moulds, forming cylinders with a 25 mm radius and 100 mm height as shown in Figure 3. The printed structure maintains stability as long as the settlement stress remains below the material's yield strength. The number of printable layers was calculated by dividing the failure height by the designed layer thickness, according to **Equations 9** and **10**.

$$h_{max} = \frac{\sigma_y}{\rho g} \quad (9)$$

$$N_{max} = \frac{h_{max}}{h_{layer}} \quad (10)$$

2.5. Thermogravimetric analysis of materials

Thermogravimetric analysis (TGA) was performed using a NETZSCH STA-499 F5 to quantify CO_2 uptake in the concrete samples. To ensure that carbonation across the entire sample was captured, a representative piece was obtained from the compression samples and ground into a fine powder. Prior to thermal analysis, the

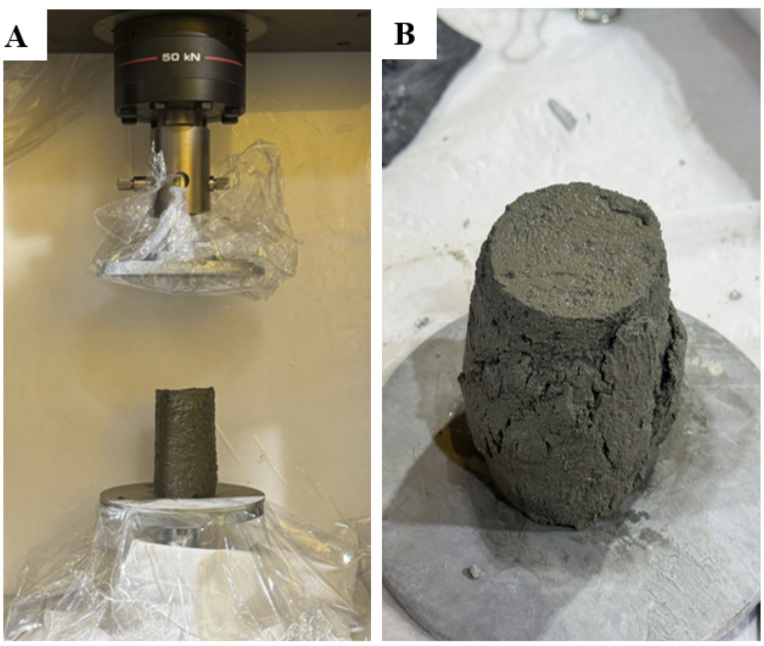

Figure 3. Uniaxial unconfined compressive test (UUCT) test of fresh-state 3D-printable materials: (A) Before failure, and (B) after failure

powdered samples were immersed in ethanol for 7–10 days to terminate hydration. This solvent exchange process effectively stops ongoing hydration by displacing pore water and denaturing hydration-active species. Following immersion, the samples were removed and dried in an oven at 60 °C for 24 hours to eliminate residual ethanol and moisture. The dried samples were then further ground into fine powders to ensure homogeneity and stored in vacuum-sealed containers until testing.

TGA was conducted by heating 1.0–1.5 g of the powdered sample from room temperature of 25 °C to 1,000 °C at a constant rate of 20 °C/min under a nitrogen atmosphere. CO_2 uptake was quantified by measuring the mass loss within the temperature range of 550 °C to 950 °C, corresponding to the thermal decomposition of carbonate phases, such as $CaCO_3$. To reflect the effectiveness of carbon capture, the results were normalized by the binder content in each mixture. All calculations assumed that the original dry mix represented the uncarbonated state of the specimen and that the influence of non-binder constituents on carbonation was negligible. The CO_2 uptake, bound water, free $Ca(OH)_2$, and degree of hydration were calculated based on standard thermal decomposition ranges and formulas reported in a recent publication.[34-36] With modifications to the original quantification method, this study followed typical temperature zones for dehydration (125–450 °C), dehydroxylation (450–550 °C), poorly crystalline $CaCO_3$ (550–750 °C), and well-crystalline $CaCO_3$ (750–950 °C), which were applied to determine the binder reaction products and carbonates. The equation for carbon uptake calculation is shown below:

$$\xi = \frac{m_{550°C} - m_{950°C}}{n \times \left(m_{125°C} - W_c - CH_f\right)} \tag{11}$$

In this equation, ξ represents carbon uptake as a weight percentage of the binder. The variable *n* denotes the weight percentage of solid binder components in the dry mix, W_c is the chemically bound water content (wt.% of the sample), and CH_f refers to the amount of free calcium hydroxide present in the sample (wt.%).

3. Results and discussion

This section presents the experimental results and corresponding discussion of 3D-printed concrete performance using coarse biochar aggregates. First, the rheological behavior of different mixtures is discussed, focusing on their effects on flowability and thixotropy, which are essential for stable extrusion in 3D printing. Next, buildability is evaluated by measuring the maximum number of printable layers and comparing these values with simulated results based on yield stress. Then, mechanical performance is discussed based on compressive and flexural strength tests at various curing ages. Finally, CO_2 uptake is assessed via TGA, highlighting the relationship between printable materials with and without biochar content.

3.1. Rheological behavior of 3D-printable biochar concrete

The rheological behaviour of the control, BC5, and BC10 mixtures was evaluated using storage modulus (G'), loss modulus (G"), and phase angle (δ). The storage modulus (G') reflects the elastic nature and early-age structural build-up of the material. As shown in Figure 4A, the control sample exhibited the highest G' values throughout the test period, suggesting stronger particle interaction and greater internal stiffness. In contrast, both biochar-modified groups exhibited lower G' values, with the 5% biochar mix (BC5) showing the greatest reduction. This indicates that biochar weakens the particle network, likely due to its porous structure and lower density. However, the 10% biochar mix (BC10) showed better recovery after deformation, as G' stabilized more quickly. This suggests that, while biochar lowers initial stiffness, it can enhance structural rebuilding by promoting rapid restructuring under rest conditions.[8]

The loss modulus (G") represents the viscous response of a material. As shown in Figure 4B, both BC5 and BC10 samples displayed higher G" values than the control, particularly in the early stages. This increase in G" suggests that incorporating biochar enhances energy dissipation and internal flowability, potentially due to the mix's looser packing and increased friction. BC10 exhibited the highest G", confirming that a greater biochar content promotes more fluid-like behavior. While this increased fluidity could facilitate extrusion during pumping, it might also compromise shape retention after deposition, thereby affecting buildability.

The phase angle δ reflects the balance between a material's elastic and viscous properties. Lower δ values indicate more solid-like behavior, while higher values suggest a more liquid-like response. As illustrated in Figure 4C, the control mix consistently exhibited the lowest δ values, indicating a predominantly elastic response and strong shape stability. Conversely, the BC5 and BC10 mixes showed higher δ values, with the BC10 mix displaying the most viscous character. Over time, δ decreased for all groups, suggesting a gradual structural recovery and increased rigidity. This recovery likely reflects the restructuring and flocculation of particles after the cessation of shear, a process crucial for maintaining the integrity of printed layers during pauses.

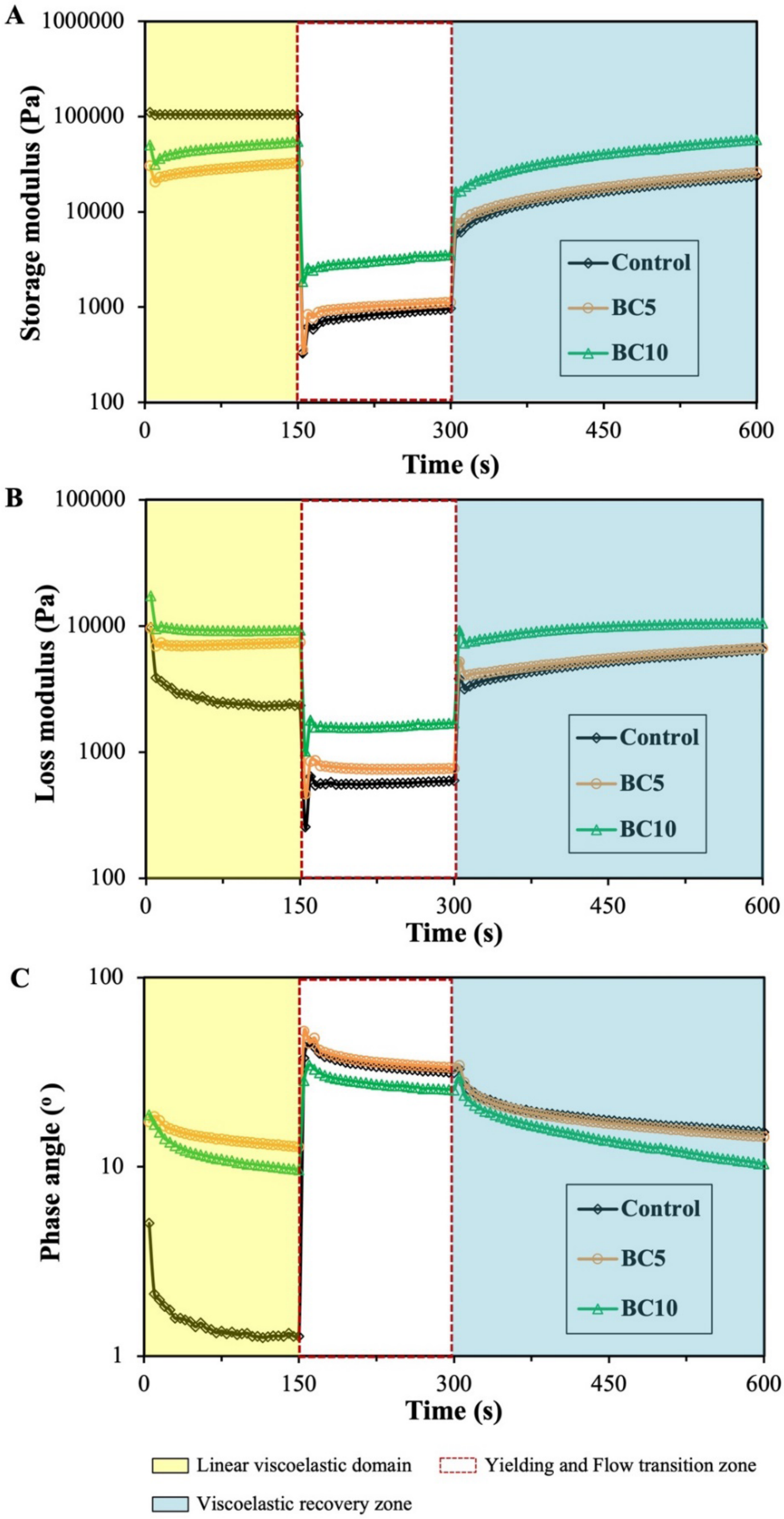

Figure 4. Effect of biochar replacement content of printable concrete for storage modulus (A), loss modulus (B), and phase angle (C)

Overall, incorporating biochar reduces the elastic stiffness and increases the viscosity of the fresh mix. This shift in rheological properties enhances extrudability and pumpability but compromises structural integrity immediately after printing. While the BC10 mix exhibits superior recovery potential, which is beneficial for continuous printing, the control sample provides the optimal balance of stiffness and shape retention. These findings underscore the importance of carefully balancing stiffness recovery, flowability, and particle interaction when formulating printable concrete mixtures with coarse biochar aggregates.

3.2. Buildability performance of 3D-printable biochar concrete

The buildability of 3D-printable concrete mixtures containing varying biochar replacement ratios was evaluated by determining the maximum number of printable layers achievable before structural failure. As illustrated in Figure 5, each mixture was printed until the subsequent layer could no longer maintain its form. Results indicate that the mixture with a 5% biochar replacement exhibited the greatest buildability, successfully printing up to 9 layers as shown in Figure 5B. The control mix achieved 7 layers, while the 10% biochar replacement mixture demonstrated the lowest buildability, collapsing after only 6 layers. As discussed previously, although the 10% biochar replacement mixture (BC10) may exhibit high fluidity, its diminished shape retention likely contributes to its reduced buildability, as evidenced in Figure 5C. The cracks observed on the surface of BC5 (Figure 5B) could be attributed to its lower fluidity, which likely caused the cement paste between the large aggregate to fracture during extrusion. Conversely, the higher fluidity of mix BC10, while not exhibiting any cracks, significantly compromised its buildability. Further research is necessary to confirm whether these cracks are solely related to mix fluidity or if printing parameters, such as print speed, also contribute. Typically, higher print speeds in 3D-printable materials with fine aggregates can stretch the layer and affect its width.[37]

The UUCT results of fresh materials exhibited a similar trend to the experimental buildability results. Specifically, the theoretical maximum printable layers were calculated from the measured yield stress, derived from the maximum compressive load obtained through UUCT. While the UUCT-based estimations accurately reflected the relative ranking of print performance, they consistently overestimated the actual print values. This discrepancy is likely due to the fact that the UUCT results were based on cast samples, which achieve better compaction and reduced air entrapment, resulting in a higher yield strength compared to the printed samples. To reconcile the UUCT-based predictions with the experimental results, a correction factor α was introduced to scale the calculated maximum printable layer number as explained in Table 2. This correction brings the theoretical values closer to the observed values, as expressed in **Equation 12**.

$$N'_{max} = \alpha \frac{h_{max}}{h_{layer}} \quad (12)$$

To ensure consistent correction and avoid overfitting, the average UUCT value was used. As demonstrated in Table 2, applying a constant factor of 0.55 to all groups significantly improves the agreement between the theoretical and experimental results.

Although, BC5 demonstrated the best buildability based on layer count; however, printing revealed practical limitations. The BC5 mixture's poor extrudability and pumpability caused printing delays and visible discontinuities. As shown in Figure 5, the BC5 sample exhibited an uneven surface and large voids in the layers. Conversely, the control and BC10 mixtures showed better extrusion consistency and fewer visible defects during printing, although the BC10 group experienced excessive extrusion, leading to material accumulation and premature structural failure.

These results suggest that while a moderate amount of

Figure 5. Number of buildable layers before failure for different printable concrete mixes. (A) Control mix for 7 layers; (B) BC5 mix for 9 layers; and (C) BC10 mix for 6 layers.

biochar (*e.g.*, 5%) can improve buildability by increasing material stiffness, it may also reduce flowability, negatively impacting overall print quality. Higher biochar content (10%), on the other hand, lowers material strength and increases the risk of over-extrusion, which negatively affects both buildability and stability. Therefore, balancing stiffness and pumpability is crucial for optimizing 3D-printable mixtures.

Table 2. Comparison of corrected theoretical buildability results with experimental results

Mix	Predicted layers	Experiment layers	α	N'_{max}
Control	12.3	7	0.55	6.8
BC5	15.4	9	0.55	8.5
BC10	11.9	6	0.55	6.5

3.3. Mechanical strength of 3D-printable biochar concrete

Figure 6 presents the compressive strength of both cast and 3D-printed samples with varying biochar replacement ratios, measured at 7 and 28 days. The cast samples were produced using the same materials as the 3D-printed samples; these materials were collected from the printer nozzle and poured into 100 m^3 cube moulds. After 7 days of curing, the control sample exhibited the highest compressive strength of 34 MPa, as shown in Figure 6A. In contrast, the BC5 and BC10 samples showed reduced early-age strength, with values of 30.9 MPa and 32.4 MPa, respectively. This initial reduction likely stems from the increased porosity and decreased packing density caused by the biochar particles, which can delay early hydration and strength development.[22] After 28 days of curing, all samples demonstrated improved strength. The BC5 sample exhibited the largest percentage increase (33.3%), reaching a compressive strength of 41.2 MPa, while the control sample increased by 19.4% to 40.6 MPa. Notably, the BC10 sample maintained the lowest compressive strength (37.0 MPa) even after extended curing.

In the printed samples as depicted in Figure 6B, the control group exhibited the highest compressive strength at 7 days (20.6 MPa), followed by BC5 (19.4 MPa) and BC10 (15 MPa). This trend mirrors that of the cast samples. The inclusion of biochar reduced early-age compressive strength, with higher replacement levels exacerbating this effect in both cast and printed concrete. At 28 days, all groups gained strength. The control samples showed the greatest increase, reaching approximately 56% above their 7 days strength. BC5 and BC10 increased by about 12% and 31%, respectively. Despite these gains, the compressive strength of both BC5 and BC10 remained significantly lower than that of the control sample.

The enhanced strength development in BC10 samples may stem from improved internal curing and gradual matrix solidification. The porous biochar aggregates likely absorb water from the mix, releasing it over time. This sustained water release could promote continued hydration and matrix densification, leading to later-age strength development. However, higher biochar content may also increase internal porosity and weaken the interfacial bond between the paste and aggregates, ultimately reducing strength, as evidenced in Figure 6.

Comparing cast and printed samples, the printed specimens consistently exhibited lower compressive strength at both curing ages. This difference primarily arises from the distinct manufacturing methods. Cast samples are compacted within the mold during pouring, facilitating air escape and improving particle packing

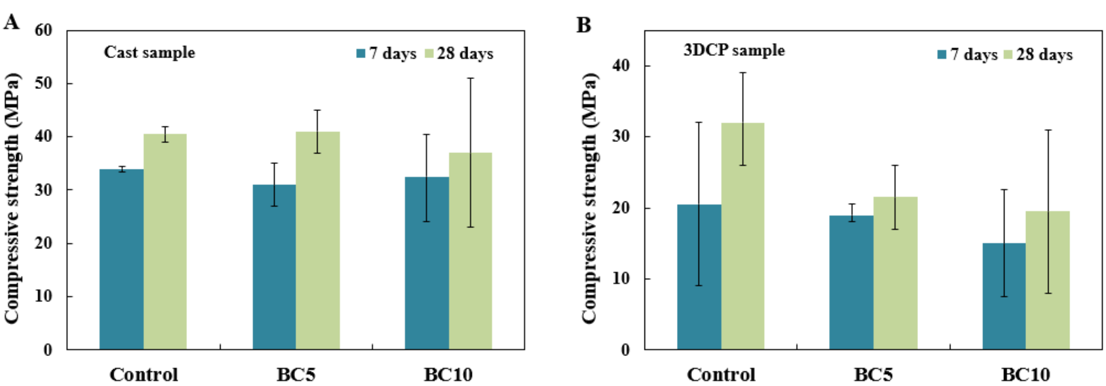

Figure 6. Compressive strength development in cast biochar concrete samples (A) and 3D-printed biochar concrete samples (B)

density. Conversely, printed samples are deposited layer by layer without vibration, resulting in higher porosity and weaker interlayer bonding. Consequently, cast samples represent the material's potential ideal strength, whereas printed samples reflect its realistic performance under additive manufacturing conditions.

The inclusion of biochar can affect the flexural strength of cementitious materials, mirroring its impact on compressive strength. Biochar's porous structure introduces voids into the matrix, decreasing overall density and causing stress to concentrate in the tension zone. These voids can act as crack initiation points, diminishing the material's resistance to bending loads and leading to a reduction in strength. The addition of excessive biochar can negatively affect the interfacial zone, potentially reducing strength.[38] Another potential reason for reduced strength with biochar addition could be exceeding the optimum limit. Most existing research on fine biochar in conventional concrete reports an optimum biochar content of approximately 2–2.5%.[18,39] At lower dosages, biochar's water absorption capacity reduces evaporable free water, thereby decreasing capillary pores. This densifies the biochar-cement microstructure and enhances the concrete's strength properties.[39] However, the filler effect and uneven surface of biochar may improve strength up to an optimal content level.[40]

Figure 7 illustrates the flexural strength development in printed samples at 7 and 28 days. At 7 days, the control samples exhibited the highest average strength at 3.9 MPa, while the BC5 and BC10 samples showed slightly lower values of 3.6 MPa and 3.7 MPa, respectively. The minimal variations and overlapping error bars among the three groups suggest that early-age flexural properties were not significantly different. After 28 days of curing, flexural strength increased in all samples. The control samples maintained the highest value, reaching 5.10 MPa. The BC5 and BC10 samples increased to 4.52 MPa and 4.16 MPa, respectively. Among the biochar-modified samples, BC5 demonstrated the greatest improvement over time (24.6%), while BC10 showed a 12.9% increase. The control group's strength increased by 31.0% from its 7-day strength. Despite the lower absolute strength values, the biochar groups exhibited a consistent upward trend. Figure 8 shows cross-sections of the fractured control, BC5 and BC10 samples after flexural testing, revealing the distribution of coarse aggregates and the presence of pores, as highlighted by circles.

Overall, biochar demonstrates promising performance in cement-based materials. However, its size, replacement content, and pyrolysis temperature require careful consideration. Research confidently concludes that incorporating an optimum content of biochar can help regulate the microstructure of the interfacial transition zone (ITZ) in cement-based composites through secondary carbonation within the pores.[41] Furthermore, the formation of a layer of calcium-rich hydration products around the biochar within the ITZ improved its connection with the hardened cement matrix.[42] This improved ITZ connection, leading to less plastic deformation in concrete with optimum biochar content, may also partially explain the observed higher strength development reported in the existing studies. Nevertheless, this phenomenon, particularly concerning coarse biochar aggregate in concrete, remains un-investigated and warrants future studies.

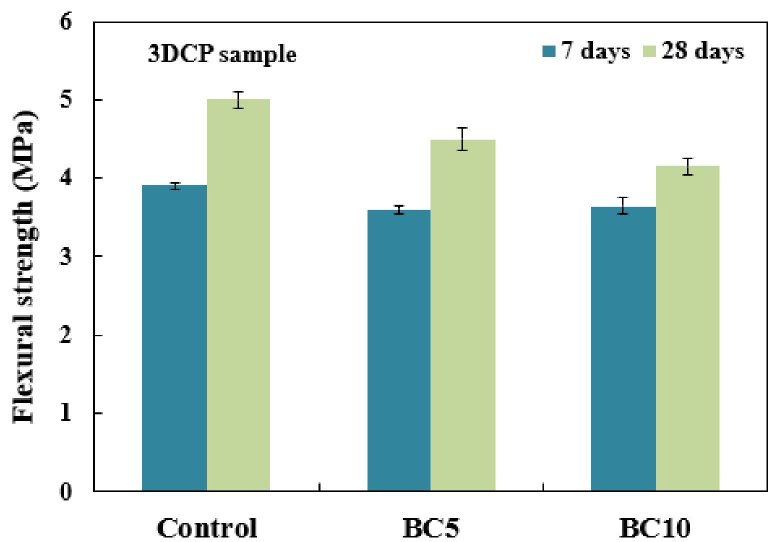

Figure 7. Flexural strength development in printed biochar concrete samples

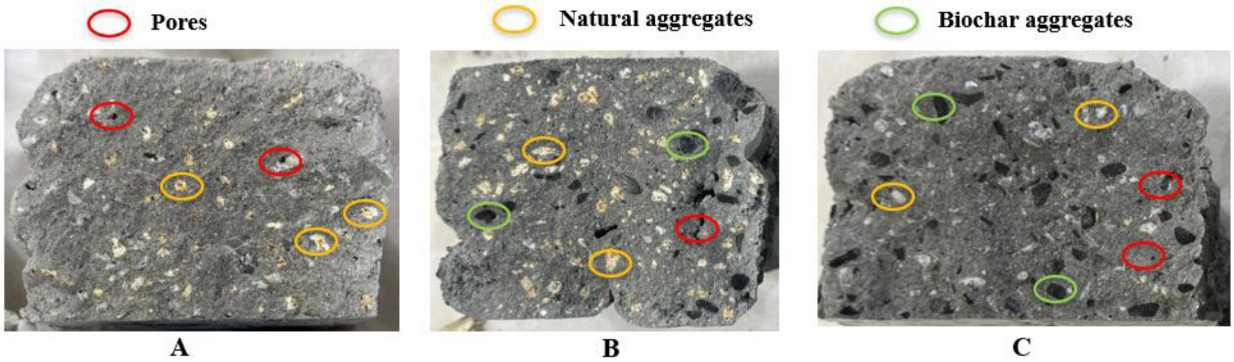

Figure 8. Cross-sections of fractured printed samples after the flexural strength test: (A) Control, (B) BC5, and (C) BC10

3.4. TGA analysis of 3D-printable biochar concrete

Figure 9 shows the TGA of mass loss at different decomposition stages across the temperature range of 25–1000 °C, along with the corresponding carbon uptake in air-cured samples after 7 days. Within the low-temperature interval (125–450 °C), each sample showed an initial weight loss associated with the removal of physically bound water and dehydration of C–S–H and AFt phases, signifying the evolution of early hydration compounds. The BC10 sample shows the highest mass loss in this range, confirming enhanced C–S–H formation attributed to internal curing provided by the porous biochar network. In the intermediate range (450–550 °C), a distinct mass loss peak is observed in all samples, representing the decomposition of portlandite ($Ca(OH)_2$) into calcium oxide and water vapor. The consistent peak position around 500 °C reflects the presence of stable and well-crystallized $Ca(OH)_2$ within the matrix. The control sample exhibits a broader thermal response in this range, indicating a more distributed $Ca(OH)_2$ phase resulting

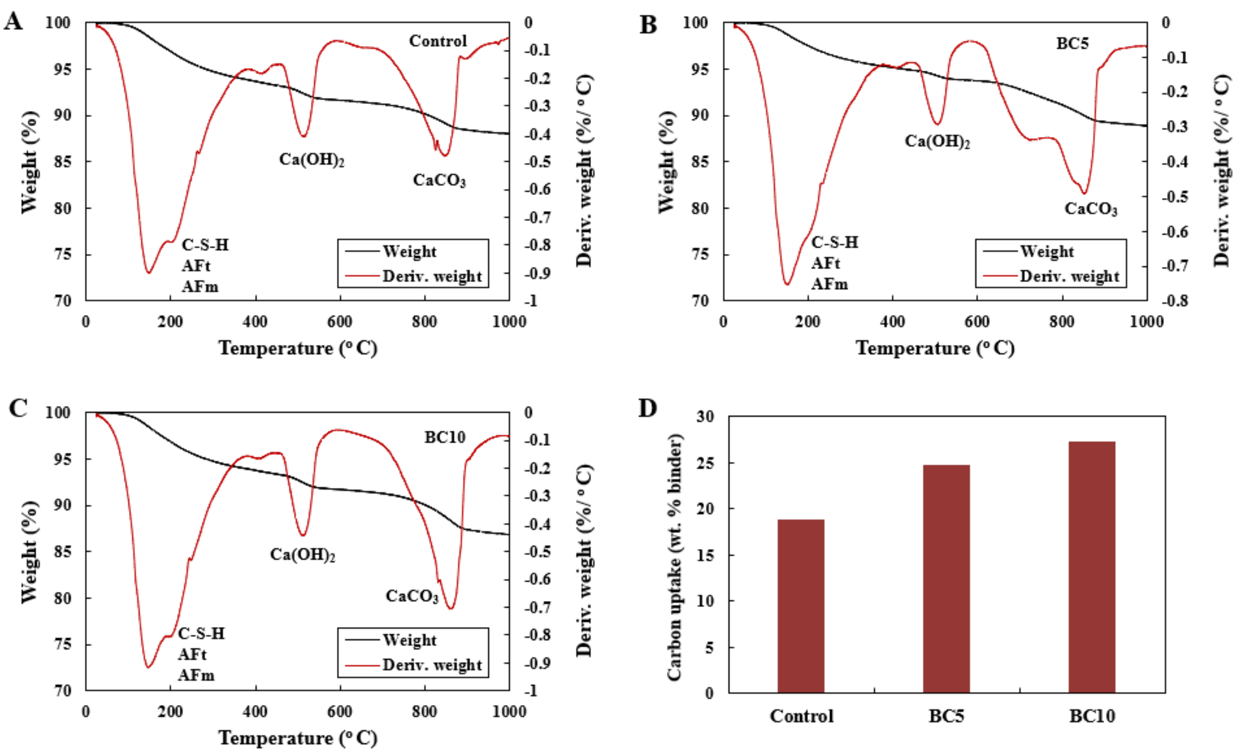

Figure 9. Thermogravimetric (TG) and derivative thermogravimetric (DTG) curves of samples control (A), BC5 (B), BC10 (C), and carbon uptake (D) after 7 days of air curing

from sustained hydration activity, while the sharper and more intense peak in the BC10 group suggests localized $Ca(OH)_2$ accumulation and limited internal moisture redistribution. In the high-temperature range (550–950 °C), mass loss is attributed to the decarbonation of calcium carbonate. The BC5 and BC10 samples show greater mass loss in this range, indicating higher CO_2 uptake and more extensive carbonation.

Biochar contributes to internal curing, supports sustained hydration, and promotes the formation of stable carbonate phases, particularly at higher replacement ratios. Compared to the control sample, BC5 shows a substantial improvement in CO_2 sequestration, and this enhancement is even more pronounced in BC10 as shown in Figure 9D. The relative increase in uptake with biochar addition reflects the role of porous carbonaceous materials in promoting carbonation under ambient curing conditions. As the biochar content increases, the matrix structure possesses more pathways for the gas diffusion and carbonate formation, resulting in more efficient long-term CO_2 storage. These results highlight the effectiveness of biochar incorporation in improving the carbon sequestration performance of 3D-printed concrete, with higher replacement levels yielding progressively greater CO_2 retention. This trend reinforces the potential of biochar as a functional additive for designing environmentally responsive construction materials.

4. Conclusions and recommendations

This study demonstrated the feasibility of using coarse biochar aggregates as a substitute for natural aggregates in carbon-responsive, 3D-printable concrete. Incorporating biochar significantly affected buildability and carbon uptake. The following conclusions are supported by this research:

(i) Regarding printability, the 5% biochar content (BC5) mix achieved the highest buildability, supporting nine printable layers before collapse a 28.6% increase compared to the control mix. The mix with 10% biochar content (BC10) exhibited the lowest buildability, supporting only six layers, suggesting an upper limit for biochar content regarding buildability.
(ii) Although the BC5 mixture supported more layers in buildability test, it exhibited reduced extrusion consistency during printing. In contrast, the control and BC10 mixes showed more stable flow behavior. These trade-offs highlight the need to balance rheological recovery, structural stiffness, and flow continuity when designing printable cementitious composites.
(iii) When comparing theoretical and experimental buildable layers, a correction factor of 0.56 improved the agreement between simulated and experimental values.
(iv) Mechanical strength tests confirmed that increasing the biochar replacement ratio decreased the compressive and flexural strength of the printed concrete. After 28 days of curing, all printed samples exhibited increased compressive strength compared to their 7-day strength: a maximum increase of 56% for control samples, and 12% and 31% increases for BC5 and BC10 samples, respectively.
(v) Carbon uptake performance was positively correlated with biochar content. Specifically, TGA after 7 days of ambient curing revealed that 5% and 10% biochar replacements enhanced CO_2 uptake by 19.5% and 45.6%, respectively, compared to the control mix.

In conclusion, while biochar reduces early strength, this study confirms that the material evolves and densifies over time, particularly at higher replacement ratios. Coarse biochar aggregates function not only as a lightweight filler but also as an active agent for *in situ* carbonation, significantly contributing to the carbon responsiveness of 3D-printed structures. However, the scarcity of research on coarse biochar replacement in both traditional and 3D-printed concrete presents a significant barrier to validating the findings presented here, necessitating further studies.

Acknowledgments

This research was supported by the Singapore Centre for 3D Printing (SC3DP) and the School of Mechanical and Aerospace Engineering (MAE) at Nanyang Technological University.

Funding

This research is funded by a charitable donation from the Mitsubishi Corporation to Nanyang Technological University, Singapore, for this project.

Conflict of interest

Suvash Chandra Paul and Ming Jen Tan serve as Guest Editors of this journal, but were not in any way involved in the editorial and peer-review process conducted for this paper, directly or indirectly. The authors declare they have no competing interests.

Author contributions

Conceptualization: Suvash Chandra Paul
Data curation: Suvash Chandra Paul
Formal analysis: Suvash Chandra Paul, Jihye Jhun, Junghyun Lee, Pengyu Chen, Yi Wei Daniel Tay

Funding acquisition: Ming Jen Tan
Investigation: Suvash Chandra Paul, Pengyu Chen, Jihye Jhun, Junghyun Lee, Yi Wei Daniel Tay
Methodology: Suvash Chandra Paul, Jihye Jhun, Junghyun Lee, Pengyu Chen
Supervision: Yi Wei Daniel Tay, Ming Jen Tan
Writing–original draft: Suvash Chandra Paul
Writing–review & editing: All authors

Ethics approval and consent to participate

Not applicable.

Consent for publication

Not applicable.

Availability of data

The datasets generated during and/or analyzed during the current study are available from the corresponding author on reasonable request.

References

1. Gibson I, Rosen D, Stucker B, Khorasani M. Development of Additive Manufacturing Technology. In: *Additive Manufacturing Technologies*. Cham, Switzerland: Springer; 2021.

   doi: 10.1007/978-3-030-56127-7_2

2. Karkun MS, Dharmalingam S. 3D printing technology in aerospace industry–a review. *IJAAA*. 2022;9(2):4.

   doi: 10.15394/ijaaa.2022.1708

3. Lai J, Wang C, Wang M. 3D printing in biomedical engineering: Processes, materials, and applications. *Appl Phys Rev*. 2021;8(2).

   doi: 10.1063/5.0024177

4. Shaukat U, Rossegger E, Schlögl S. A review of multi-material 3D printing of functional materials via vat photopolymerization. *Polymers*. 2022;14(12):2449.

   doi: 10.3390/polym14122449

5. Nachal N, Moses JA, Karthik P, Anandharamakrishnan C. Applications of 3D printing in food processing. *Food Eng Rev*. 2019;11(3):123-141.

   doi: 10.1007/s12393-019-09199-8

6. Pan Y, Zhang Y, Zhang D, Song Y. 3D printing in construction: state of the art and applications. *Int J Adv Manuf Technol*. 2021;115(5):1329-1348.

   doi: 10.1007/s00170-021-07213-0

7. Žujović M, Obradović R, Rakonjac I, Milošević J. 3D printing technologies in architectural design and construction: A systematic literature review. *Buildings*. 2022;12(9):1319.

   doi: 10.3390/buildings12091319

8. Paritala S, Singaram KK, Bathina I, Khan MA, Jyosyula SKR. Rheology and pumpability of mix suitable for extrusion-based concrete 3D printing–A review. *Constr Build Mater*. 2023;402:132962.

   doi: 10.1016/j.conbuildmat.2023.132962

9. Sun Y, Zhang X, Zhou J, *et al*. Extrudability analysis of 3D printable concrete as a two-phase discrete flow. *J Build Eng*. 2024;98:111252.

   doi: 10.1016/j.jobe.2024.111252

10. Xia Z, Geng J, Zhou Z, Liu G. Comparative analysis of polypropylene, basalt, and steel fibers in 3D printed concrete: Effects on flowability, printability, rheology, and mechanical performance. *Constr Build Mater*. 2025;465:140098.

    doi: 10.1016/j.conbuildmat.2025.140098

11. Ivanova I, Ivaniuk E, Bisetti S, Nerella VN, Mechtcherine V. Comparison between methods for indirect assessment of buildability in fresh 3D printed mortar and concrete. *Cem Concr Res*. 2022;156:106764.

    doi: 10.1016/j.cemconres.2022.106764

12. He Z, Zhu X, Wang J, Mu M, Wang Y. Comparison of CO2 emissions from OPC and recycled cement production. *Constr Build Mater*. 2019;211:965-973.

    doi: 10.1016/j.conbuildmat.2019.03.289

13. Ige OE, Von Kallon DV, Desai D. Carbon emissions mitigation methods for cement industry using a systems dynamics model. *Clean Technol Environ Policy*. 2024;26(3):579-597.

    doi: 10.1007/s10098-023-02683-0

14. Lehmann J, Cowie A, Masiello CA, *et al*. Biochar in climate change mitigation. *Nat Geosci*. 2021;14(12):883-892.

    doi: 10.1038/s41561-021-00852-8

15. Suarez-Riera D, Restuccia L, Ferro GA. The use of Biochar to reduce the carbon footprint of cement-based materials. *Procedia Struct Integr*. 2020;26:199-210.

    doi: 10.1016/j.prostr.2020.06.023

16. Gupta S, Kua HW, Dai Pang S. Effect of biochar on mechanical and permeability properties of concrete exposed to elevated temperature. *Constr Build Mater*. 2020;234:117338.

    doi: 10.1016/j.conbuildmat.2019.117338

17. Gupta S, Kua HW. Effect of water entrainment by pre-soaked biochar particles on strength and permeability of cement mortar. *Constr Build Mater*. 2018;159:107-125.

    doi: 10.1016/j.conbuildmat.2017.10.095

18. Sirico A, Belletti B, Bernardi P, *et al*. Effects of biochar addition on long-term behavior of concrete. *Theor Appl Fract Mech*. 2022;122:103626.

    doi: 10.1016/j.tafmec.2022.103626

19. Chen L, Zhu X, Zheng Y, Wang L, Poon CS, Tsang DC. Development of high-strength lightweight concrete by utilizing food waste digestate based biochar aggregate. *Constr Build Mater*. 2024;411:134142.

doi: 10.1016/j.conbuildmat.2023.134142

20. Song S, Liu Z, Liu G, Cui X, Sun J. Application of biochar cement-based materials for carbon sequestration. *Constr Build Mater*. 2023;405:133373.

doi: 10.1016/j.conbuildmat.2023.133373

21. Wyrzykowski M, Toropovs N, Winnefeld F, Lura P. Cold-bonded biochar-rich lightweight aggregates for net-zero concrete. *J Clean Prod*. 2024;434:140008.

doi: 10.1016/j.jclepro.2023.140008

22. Park JH, Lim KM, Ryu GS, Koh KT, Kim KC. An experimental study on the thermal insulation properties of concrete containing wood-based biochar. *Appl Sci*. 2025;15(19):10560.

doi: 10.3390/app151910560

23. Revathi S, Alice Elizabeth Tania D, Ancy Shadin S, Keerthana J. Effect of zeolite and bamboo biochar as CO2 absorbant in concrete. *Carbon Res*. 2024;3(1):43.

doi: 10.1007/s44246-024-00116-1

24. Zhou Y, Wang S, Chen L. Progress and prospects of biochar as concrete filler: A review. *Alex Eng J*. 2025;128:306-323.

doi: 10.1016/j.aej.2025.05.077

25. Zhang C, Zhang J, Su Y, *et al*. Low-carbon 3D-printed concrete by using biochar as a carbon sequestrator. In: *Biochar-Based Cement and Concrete for Sustainable Construction*. Cambridge, UK: Woodhead Publishing; 2026:67-88.

doi: 10.1016/B978-0-443-22037-1.00009-4

26. Vergara LA, Perez JF, Colorado HA. 3D printing of ordinary Portland cement with waste wood derived biochar obtained from gasification. *Case Stud Constr Mater*. 2023;18:e02117.

doi: 10.1016/j.cscm.2023.e02117

27. Jhun J, Lee J, Paul SC, *et al*. Potential of rice husk biochar in 3D concrete printing: an analysis of fresh-state rheology, strength retention, and carbon sequestration. *Virtual Phys Prototyp*. 2026;21(1):e2619391.

doi: 10.1080/17452759.2026.2619391

28. Praneeth S, Guo R, Wang T, Dubey BK, Sarmah AK. Accelerated carbonation of biochar reinforced cement-fly ash composites: enhancing and sequestering CO2 in building materials. *Constr Build Mater*. 2020;244:118363.

doi: 10.1016/j.conbuildmat.2020.118363

29. Chen Y, Zhan B, Guo B, *et al*. Biochar-enhanced cement composites as carbon sink under accelerated carbonation curing: Carbon sequestration potential stimulated by biochar porosity. *Constr Build Mater*. 2025;492:143005.

doi: 10.1016/j.conbuildmat.2025.143005

30. Dixit A, Gupta S, Dai Pang S, Kua HW. Waste Valorisation using biochar for cement replacement and internal curing in ultra-high performance concrete. *J Clean Prod*. 2019;238:117876.

doi: 10.1016/j.jclepro.2019.117876

31. De Guzman AIR, Mateo WC, Denson MD, Villota EM, Perez MG. Synthesis and evaluation of rice straw-derived biochar as cement replacement for concrete. *J Build Eng*. 2025:113617.

doi: 10.1016/j.jobe.2025.113617

32. Harbouz I, Roziere E, Yahia A, Loukili A. Printability assessment of cement-based materials based on rheology, hydration kinetics, and viscoelastic properties. *Constr Build Mater*. 2022;325:126810.

doi: 10.1016/j.conbuildmat.2022.126810

33. Wang H, Zentar R, Wang D. Rheological characterization of fine-grained sediments under steady and dynamic conditions. *Int J Geomech*. 2022;22(1):04021260.

doi: 10.1061/(ASCE)GM.1943-5622.0002243

34. Bhatty JI. Hydration versus strength in a Portland cement developed from domestic mineral wastes—a comparative study. *Thermochim Acta*. 1986;106:93-103.

doi: 10.1016/0040-6031(86)85120-6

35. Dixit A, Du H, Dai Pang S. Carbon capture in ultra-high performance concrete using pressurized CO2 curing. *Constr Build Mater*. 2021;288:123076.

doi: 10.1016/j.conbuildmat.2021.123076

36. Lim SG, Tay YWD, Paul SC, *et al*. Carbon capture and sequestration with in-situ CO2 and steam integrated 3D concrete printing. *Carbon Capture Sci Technol*. 2024;13:100306.

doi: 10.1016/j.ccst.2024.100306

37. Panda B, Paul SC, Mohamed NAN, Tay YWD, Tan MJ. Measurement of tensile bond strength of 3D printed geopolymer mortar. *Measurement*. 2018;113:108-116.

doi: 10.1016/j.measurement.2017.08.051

38. Scrivener KL, Crumbie AK, Laugesen P. The interfacial transition zone (ITZ) between cement paste and aggregate in concrete. *Interface Sci*. 2004;12(4):411-421.

doi: 10.1023/B:INTS.0000042339.92990.4c

39. Patel R, Stobbs J, Acharya B. Study of biochar in cementitious materials for developing green concrete composites. *Sci Rep*. 2025;15(1):22192.

doi: 10.1038/s41598-025-07210-3

40. Ali D, Agarwal R, Hanifa M, *et al*. Thermo-physical properties

and microstructural behaviour of biochar-incorporated cementitious material. *J Build Eng*. 2023;64:105695.

doi: 10.1016/j.jobe.2022.105695

41. Xu W, Li M, Liang J, *et al*. Microstructural regulation of interfacial transition zone by biochar: A novel strategy for enhancing fire resistance. *Cem Concr Compos*. 2026;169:106517.

doi: 10.1016/j.cemconcomp.2026.106517

42. Zhu X, Zhang Y, Chen L, *et al*. Bonding mechanisms and micro-mechanical properties of the interfacial transition zone (ITZ) between biochar and paste in carbon-sink cement-based composites. *Cem Concr Compos*. 2023;139:105004.

doi: 10.1016/j.cemconcomp.2023.105004